# PRACTICAL CONSIDERATIONS ON PROPRIOCEPTIVE TACTILE SENSING FOR UNDERACTUATED FINGERS

Bruno Belzile[1], Lionel Birglen[1]
[1]*Department of Mechanical Engineering, Polytechnique Montréal, Montréal, Québec, Canada*
*Email: bruno.belzile@polymtl.ca; lionel.birglen@polymtl.ca*

## ABSTRACT

Underactuation is becoming more prevalent in the design of new robotic graspers to replace humans in laborious, dangerous, and repetitive tasks. The use of such mechanisms is motivated by the desire to reduce the complexity and associated costs of conventional fully actuated systems. Furthermore, to accomplish several tasks with artificial hands, tactile sensing is often required to assess the grasp stability and to control the contact forces applied. With the same objective of reducing the costs of the components needed to provide this sensory feedback, several authors have worked on finding alternatives to external tactile sensors. This paper is about one of these methods, namely proprioceptive tactile sensing, especially designed for underactuated fingers. It focuses on certain practical considerations, such as the impact of the curvature of the grasped object and the reconfiguration of the finger after the contact, and proposes the analysis of their influence on the precision of the algorithm. To this aim, simulations and experimental data are provided for different grasping scenarios.

**Keywords:** tactile sensing; underactuation; kinematics; grasping.

# CONSIDÉRATIONS PRATIQUES SUR LA MESURE TACTILE PROPRIOCEPTIVE POUR DES DOIGTS SOUS-ACTIONNÉS

## RÉSUMÉ

Le sous-actionnement devient de plus en plus répandu dans la conception de nouveaux préhenseurs robotiques, et ce, dans l'optique de remplacer les humains dans le cadre de tâches laborieuses, dangereuses et répétitives. Le choix de ce type de mécanismes est motivé par le désir de réduire la complexité et les coûts associés aux systèmes classiques pleinement actionnés. Pour de nombreuses applications, la rétroaction tactile est de plus nécessaire pour connaître la stabilité de la saisie et ajuster les forces de contact appliquées. Afin d'également réduire les coûts associés aux composants nécessaires pour établir un retour sensoriel, plusieurs auteurs ont travaillé à trouver des solutions alternatives aux capteurs externes conventionnels. Cet article porte sur une de ces méthodes, à savoir la mesure tactile proprioceptive, cette dernière étant conçue spécifiquement pour les préhenseurs sous-actionnés. Un intérêt particulier est porté sur certaines considérations pratiques, soit l'effet de la courbure de l'objet saisi et la reconfiguration après le contact, le tout en lien avec la précision de l'algorithme proposé. Pour ce faire, des simulations et des tests expérimentaux sont effectués pour différents contacts. Il a pu être constaté que la courbure locale de l'objet, bien qu'ayant un effet en théorie, n'a qu'un impact marginal par rapport à d'autres causes d'imprécision telles que le frottement. De plus, il est aussi démontré que, dans des limites raisonnables, la reconfiguration après le contact nécessaire à l'estimation tactile ne cause pas de grandes déviations sur l'estimation de la position du contact.

**Mots-clés :** mesure tactile ; sous-actionnement ; cinématique ; saisie.

## NOMENCLATURE

| | |
|---|---|
| $T_a$ | actuation torque at the base of the finger |
| $\Delta T_a$ | actuation torque increase to have the reconfiguration of the finger needed for the estimation |
| $\theta_a$ | actuation angle at the base of the transmission mechanism |
| $\boldsymbol{\theta}$ | interphalangeal relative angles |
| $\mathbf{x}$ | transmission vector |
| $K_c$ | instantaneous stiffness |
| $\mathbf{K}$ | stiffness matrix |
| $\mathbf{J}$ | Jacobian matrix |
| $\mathbf{J}_i^*$ | reduced Jacobian matrix |
| $\mathbf{G}$ | product of the mathematical jacobian of $\mathbf{x}$ with respect of $\boldsymbol{\theta}$ and the actuation torque $T_a$ |
| $k_i$ | contact location on the $i^{\text{th}}$ phalanx |
| $\boldsymbol{\tau}$ | total torques at the interphalangeal joints |
| PTS | proprioceptive tactile sensing |
| | |
| Subscripts | |
| $i$ | $i^{\text{th}}$ phalanx |
| $c$ | instant of contact |

## 1. INTRODUCTION

Robotic grippers and hands have become prevalent in many fields. In a foreseeable future, they are expected to replace human manipulation for a large variety of repetitive tasks, especially when robots become more precise and efficient. Moreover, robotic graspers can lift heavier loads and accomplish maneuvers humans could not. They are particularly useful to manipulate objects in hostile environments without endangering humans. Therefore, a lot of work has been done in recent years to improve their capabilities such as their speed, dexterity, strength, and versatility. However, current robotic manipulators often lack the sensory feedback of their human counterparts. Indeed, haptic and tactile feedback is still very limited in current robotic systems, which leads to several limitations since tactile sensing is deemed nearly mandatory for a significant number of applications. Conventional tactile sensors, which are attached on the external surface of a robot, can generally be used, but they are often costly, insensible to dynamic phenomena, and inadequate in certain applications [1, 2].

To solve those issues, many authors have investigated alternatives to standard tactile sensors. For instance, intrinsic sensors instead of extrinsic ones have been proposed. The former measures forces within the grasping mechanism whereas extrinsic sensors measure forces that act upon the mechanism [3]. As an example of intrinsic tactile sensing, in [4], the authors used a 6-axis force/torque sensor built in the interior of the fingertip, avoiding having any sensor on the finger's surface. On the other hand, exteroceptive sensors can also be used as an alternative to conventional pressure-based tactile sensors. Indeed, the authors of [5] have designed a method to detect a contact on a compliant underactuated finger using an accelerometer. With a phase-locked loop circuit vibrating the linkage, they were able to locate the contact by measuring the changes in the resonance frequency of the finger. Moreover, geometric relationships can also be used to estimate contact locations, as in [6] and [7] with position and torque sensors in the joints. In [8], passive displacements of joints with compliance was used to estimate the location of an incidental collision with three different techniques, namely a closed-form inference model based on a serial chain with joint springs, a variation on Self-Posture Changeability as proposed by [9], and an empirical memory-based model of joint trajectories. In most of these cases, internal sensors were used with fully actuated mechanisms.

This paper is part of this search for viable alternatives to conventional tactile solutions and focuses on the possibility of using the stiffness perceived at the actuator of an underactuated finger to perform tactile

| 2-DOF S-class | | | |
|---|---|---|---|
| $l_1$ | 10 cm | $c$ | 4.4 cm |
| $l_2$ | 7.5 cm | $\theta_{0,2}$ | 0 rad |
| $a$ | 7.1 cm | $\theta_{0,1}$ | $\pi/4$ rad |
| $b$ | 10.8 cm | $\phi_2$ | $\pi/2$ rad |

Table 1. Geometric parameters of the prototype

sensing. This technique is referred to as proprioceptive tactile sensing (PTS), as no exteroceptive sensor is needed. It is applied here to underactuated robotics fingers, which are becoming increasingly common. Underactuated mechanisms, sometimes referred to as self-adaptive, are particularly interesting because of their intrinsic ability to mechanically adapt themselves to the shape of an object without complex control laws and using as few as only one actuator. A transmission mechanism and compliant elements are used to constrain the motion and provide shape adaptation. Linkages and tendons are commonly used to distribute the actuation torque (or force) to the phalanges [10]. As these mechanisms have by definition fewer actuators, they generally have no sensor in the finger's mechanism itself. Instead of adding new sensors, it is possible to take advantage of the sensors already present, such as the ones at the actuator, namely optical encoders and current/voltage sensors. With those sensors, it is possible to measure the variation of the overall stiffness as seen at the actuator. This stiffness being a function of the compliance of the mechanism and the applied contact forces, it is possible to estimate the contact locations solely from the measurements at the actuator. Several authors have worked on taking advantage of the internal stiffness of underactuated mechanisms, but it was mostly done to improve the stability and adjust the type of grasp [11].

This paper continues the work presented in [12], where a complete model of the stiffness of an underactuated finger as seen at the actuator was presented with an algorithm to estimate the initial contact location. Going a step further, practical considerations such as the curvature of the object and the input torque variation needed to estimate the contact location are analyzed in this paper.

## 2. PROPRIOCEPTIVE TACTILE SENSING

### 2.1. Initial Considerations

Proprioceptive tactile sensing is a method in which the estimation of the contact point on an underactuated finger relies on the measured instantaneous stiffness at the sole actuator. The latter is defined as:

$$K_c = dT_a/d\theta_a \approx \Delta T_a/\Delta\theta_a = \frac{T_{a,f} - T_{a,0}}{\theta_{a,f} - \theta_{a,0}}, \tag{1}$$

where $T_a$ and $\theta_a$ are respectively the input torque and position measured at the actuator. The object with which the underactuated finger makes contact is assumed immovable and completely rigid. Contact friction is neglected and the unique initial contact force is then assumed normal to the surface of its associated phalanx. As detailed in [12], precise contact localization can only be done for contacts made after the proximal phalanx. The geometry of the finger used in this paper is shown in Fig. 1. The numerical values of the parameters used in the examples are given in Table 1.

### 2.2. Method

As proven in [12], the inverse of the instantaneous stiffness of an underactuated finger at the instant of the initial contact can be computed with the following equation:

$$K_c^{-1} = \mathbf{x}\mathbf{A}^{-1}\mathbf{B}\mathbf{x}, \tag{2}$$

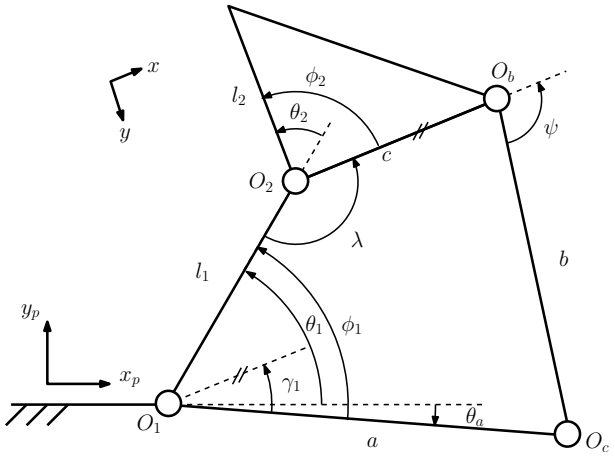


Fig. 1. Geometry of the 4-bar linkage-driven transmission

with

$$\mathbf{A} = \begin{bmatrix} \mathbf{J}_i^*(\mathbf{K}-\mathbf{G}) \\ \mathbf{\Gamma}_i^T \end{bmatrix} \quad \text{and} \quad \mathbf{B} = \begin{bmatrix} \mathbf{J}_i^* \\ \mathbf{0}^T \end{bmatrix}. \tag{3}$$

The diagonal matrix $\mathbf{K}$ contains the stiffness coefficients of the compliant elements located at the interphalangeal joints. The vector $\mathbf{\Gamma}_i$ contains coefficients that are functions of the phalanx in contact and location of the latter. The matrix $\mathbf{J}_i^*$ is a reduced Jacobian linking the torques at the interphalangeal joints to the normal contact forces applied at the phalanges, and $\mathbf{G}$ is the product of the mathematical Jacobian of the vector $\mathbf{x}$ (transmission factors, see [12]) with respect to the interphalangeal angles $\theta_i$ and the actuation torque $T_a$. For a two-phalanx finger such as the one analyzed in this paper, $\mathbf{J}_i^*$ is defined for an initial contact on the proximal or distal phalanx as either:

$$\mathbf{J}_1^* = \begin{bmatrix} 0 & 1 \end{bmatrix} \quad \text{or} \quad \mathbf{J}_2^* = \begin{bmatrix} 1 & -\beta_2 \end{bmatrix}, \tag{4}$$

respectively, and where

$$\beta_2 = 1 + (l_1 \cos\theta_2)/k_2. \tag{5}$$

The variable $k_i$ is the distance between the lower joint of a phalanx and the contact location. The subscript 2 refers to the distal phalanx in Fig. 1. The transmission vector $\mathbf{x}$ is defined for a 2-DOF finger as:

$$\mathbf{x} = \begin{bmatrix} x_1 & x_2 \end{bmatrix}, \tag{6}$$

where the different $x_i$ are a function of the transmission mechanism used and its parameters. In the case of a linkage-driven transmission mechanism as shown in Fig. 1, these variables are defined as:

$$x_1 = 1, \quad x_2 = z/(l_2 - z), \tag{7}$$

with

$$z = \frac{ac\sin(\pi - \theta_1 + \theta_a - \lambda) - l_1 c \sin\lambda}{a\sin(\pi - \theta_a + \theta_a) - c\sin\lambda}. \tag{8}$$

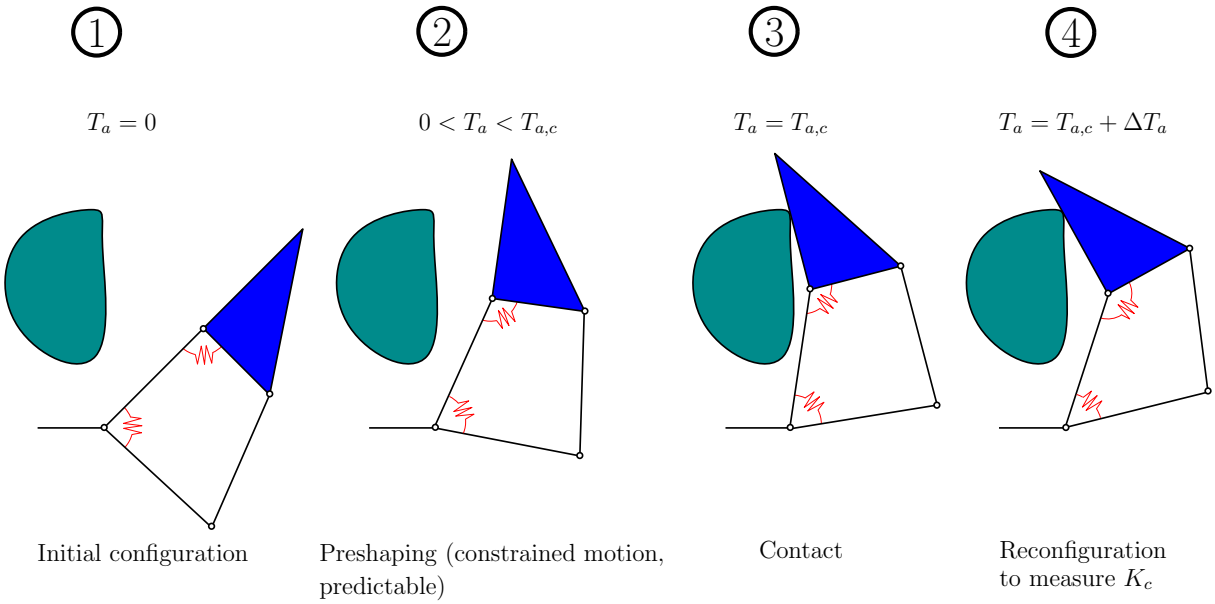


Fig. 2. Proprioceptive Tactile Sensing

### 2.3. Reconfiguration after the Contact

To be able to estimate the contact location along the distal phalanx, a reconfiguration of the finger after the contact is needed to be able to compute the instantaneous stiffness as seen at the actuator. Indeed, a variation of $\theta_a$ and $T_a$ must be measured to use Eq. (2). This shape adaptation is naturally caused by an increase of the actuation torque $\Delta T_a$. The value of the latter is arbitrarily chosen, and thus, has an impact on the algorithm's output, as it depends on the reconfiguration of the finger. This element, alongside the effect of the object's curvature at the point of contact, will be analyzed in Section 3.2. A conceptual representation of how proprioceptive tactile sensing works is shown in Fig. 2.

### 2.4. Experimental Setup

To validate the findings of the simulations and the theoretical model, a gripper made of two 2-DOF linkage-driven fingers was used (shown in Fig. 3). The parameters of these fingers correspond to these listed in Table 1. Both fingers are actuated independently by a Maxon RE10 DC motor. Gears, pulleys, and a nylon cable transmit the actuation torque to the base link $O_1O_c$. Springs are located in joints $O_1$ and $O_2$.

## 3. ANALYSIS OF A CONTACT ON A CURVED SURFACE

When grasping a practical object, it is not unusual to come into contact with a curved surface. Therefore, it would be interesting to assess the effect of this curvature on the estimation accuracy of the PTS algorithm presented in [12]. Indeed, while in theory it does not have any effect as the method is based on an instantaneous value of the stiffness at the actuator, in practice, the motion after contact needed to make the estimation is influenced by the curvature of the object.

### 3.1. Kinetostatic Analysis

Using the virtual work principle, one can compute the trajectory and the variation of stiffness caused by a curved surface. As presented in [13], a set of equations can be established. For a 2-DOF linkage-driven

Fig. 3. Experimental setup

transmission with torsional springs at the interphalangeal joints, one has:

$$\delta W = -\sum_{i=1}^{2} K_i \Delta\theta_i \delta\theta_i - T_a \delta\theta_a - \sum_{i=1}^{2} \mathbf{f}_i{}^T \delta\mathbf{z}_i. \tag{9}$$

In Eq. (9), $\mathbf{f}_i{}^T \delta\mathbf{z}_i$ is the virtual work done by the $i^{\text{th}}$ contact force. The vector $\mathbf{z}_i$ is defined as going from the origin of the reference frame to the associated contact point. The coefficients $K_i$ are the diagonal elements of the stiffness matrix $\mathbf{K}$. Therefore, one has:

$$\mathbf{f}_1{}^T \delta\mathbf{z}_1 = ||\mathbf{f}_1|| k_1 \delta\theta_1, \tag{10}$$

$$\mathbf{f}_2{}^T \delta\mathbf{z}_2 = ||\mathbf{f}_2|| \left(l_1 \cos\theta_2 \delta\theta_1 + k_2 \delta(\theta_1 + \theta_2)\right). \tag{11}$$

By differentiating Eq. (9) with respect to the two interphalangeal relative joint angles $\theta_i$, one obtains two equations. To be able to solve this system of two equations, additional relationships are needed since there are five unknowns, namely the configuration variables of the finger ($\theta_a$, $\theta_1$, $\theta_2$) and the Cartesian location of the contact point ($X_p$, $Y_p$). One of the additional relationships is the expression of $\theta_a$ as a function of $\theta_1$ and $\theta_2$. If one considers the four-bar linkage of the transmission mechanism (shown in Fig. 1), one has:

$$\boldsymbol{r}_1 = \overrightarrow{O_2O_1} = l_1 \begin{bmatrix} \cos\lambda \\ \sin\lambda \end{bmatrix}, \; \boldsymbol{r}_2 = \overrightarrow{O_1O_c} = a \begin{bmatrix} \cos\gamma \\ \sin\gamma \end{bmatrix}, \tag{12}$$

$$\boldsymbol{r}_3 = \overrightarrow{O_2O_b} = c \begin{bmatrix} 1 \\ 0 \end{bmatrix}, \; \boldsymbol{r}_4 = \overrightarrow{O_bO_c} = b \begin{bmatrix} \cos\psi \\ \sin\psi \end{bmatrix}. \tag{13}$$

By expressing $\boldsymbol{r}_4$ as a function of the other $\boldsymbol{r}_i$ and computing its norm, the following is obtained:

$$||\boldsymbol{r}_4|| = ||\boldsymbol{r}_1 + \boldsymbol{r}_2 - \boldsymbol{r}_3||. \tag{14}$$

Using Eqs. (12) and (13), this last expression can be rewritten as:

$$\zeta_1 - \zeta_2 \cos\gamma_i - \zeta_3 \cos\lambda + \cos(\gamma - \lambda) = 0, \tag{15}$$

where

$$\zeta_1 = (l_1^2 + c^2 + a^2 - b^2)/(2al_1),\ \zeta_2 = c/l_1,\ \zeta_3 = c/a. \tag{16}$$

After simplification, Eq. (15) becomes:

$$A\cos\gamma + B\sin\gamma + C = 0, \tag{17}$$

where

$$A = \cos\lambda - \zeta_2,\ B = \sin\lambda,\ C = \zeta_1 - \zeta_3\cos\lambda. \tag{18}$$

By defining $T_i = \tan(\gamma/2)$, a quadratic form is obtained:

$$D(\lambda)T^2 + E(\lambda)T + F(\lambda) = 0, \tag{19}$$

where

$$D = C - A,\ E = 2B,\ F = A + C. \tag{20}$$

By computing the inverse tangent of the roots of Eq. (19), one obtains an expression of $\gamma$ as a function of $\lambda$, and with

$$\lambda = \pi + \theta_2 - \phi_2 \quad \text{and} \quad \theta_a = \theta_1 - \gamma_i, \tag{21}$$

an expression $\theta_a = g(\theta_1, \theta_2)$ is then obtained. Finally, the system of equations becomes fully determined by adding the geometric closure equations of the contact location. While the latter depends on the $(X_p - Y_p)$ curve defining the object (its shape in the plane), one has:

$$X_p = \begin{cases} k_1\cos\theta_1 & \text{if the contact occurs on the proximal phalanx,} \\ l_1\cos\theta_1 + k_2\cos(\theta_1+\theta_2) & \text{if the contact occurs on the distal phalanx,} \end{cases} \tag{22}$$

and

$$Y_p = \begin{cases} k_1\sin\theta_1 & \text{if the contact occurs on the proximal phalanx,} \\ l_1\sin\theta_1 + k_2\sin(\theta_1+\theta_2) & \text{if the contact occurs on the distal phalanx.} \end{cases} \tag{23}$$

With these equations, it is possible to completely simulate the behavior of an underactuated finger and its adaptation to the shape of a curved object.

### 3.2. Simulations

Simulations were performed with cylinders of different radii, cf. the example shown in Fig. 4. These simulation results were also validated with a dynamic simulation package (DSP). The data obtained shows that the curvature of the surface can have an impact on the estimation of the PTS algorithm. Indeed, the deviation of the estimated stiffness compared to its actual value depends on the amount of the torque increase $\Delta T_a$ chosen and used by the algorithm, more precisely by Eq. (1). A $\Delta T_a$ too small makes the algorithm sensitive to measurement noise, while a $\Delta T_a$ too large makes the estimation imprecise in the case of a non-vertex point of contact. A large $\Delta T_a$ also makes the finger prone to a second contact on the object.

In the illustrated example, for an initial contact at $k_2 = 2.927$ cm, the instantaneous stiffness is measured by the algorithm after a torque increase $\Delta T_a = 0.8$ N (arbitrary chosen) that resulted in a 0.08 rad variation of $\theta_a$. The theoretical value of $K_c$ for this contact is 6.725 Nm/rad. With the previously mentioned motion after contact needed to measure the instantaneous stiffness, the computed value of $\hat{K}_c$ is 9.965 Nm/rad, resulting in an estimated location of contact $\hat{k}_2 = 4.153$ cm, i.e. an error of 16.3 % relative to the length of the phalanx. The original and final configurations are respectively shown by dashed and solid lines on the left-hand side of Fig. 4. This can be explained by the fact that the contact point moves toward a point located beyond the end of the phalanx in this case. While there is a discrepancy between the theoretical and measured values of

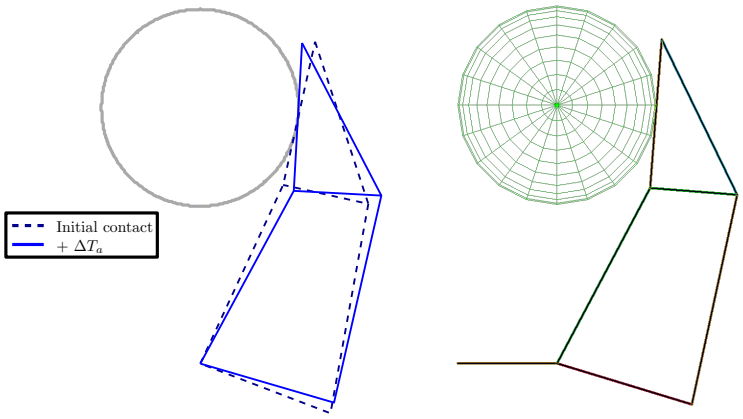


(a) Numerical simulation (b) Dynamic simulation package

Fig. 4. Representation of the contact configuration, including the reconfiguration needed to estimate the point of contact

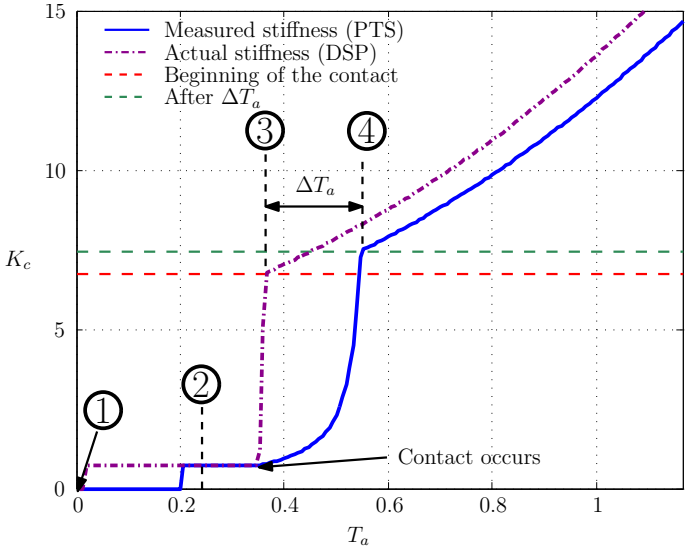


Fig. 5. Simulated signals for a contact on a curved object

$K_c$ in this particular example, the estimated location of $k_2$ is near the new location of the contact point after the measurement reconfiguration, namely 3.941 cm. Simulated signals showing how the algorithm works are illustrated in Fig. 5, see Fig. 2 for an illustration of the numbered phases.

In this figure, the two curves show the evolution of the theoretical instantaneous stiffness ($K_c$, dashed-dotted curve) and the one measured and used by the PTS algorithm ($\hat{K}_c$, solid). All the data is obtained with the DSP (data obtained with the theoretical model was nearly identical to the one of the DSP, and thus is not shown for clarity). The inputs and output of the PTS algorithm are respectively the measurements at the actuator ($\theta_a$, $T_a$) and the estimation of the contact location. The estimated $\hat{K}_c$, illustrated in Fig. 5, is an intermediate result. From this figure, several elements can be pointed out. First, it can be seen that there is an horizontal shift between both curves (from step 3 in Fig. 2, the moment contact occurs, to step 4, after the arbitrarily chosen $\Delta T_a$), which is due to the amount of torque increase applied to obtain a reconfiguration of the finger and be able of computing the instantaneous stiffness. Furthermore, this interval also has an

impact on the measured instantaneous stiffness itself and its evolution. Indeed, because the value used in the algorithm is in practice not instantaneous, it is not exactly the same as it should theoretically be. Also, it can be seen that the shift that occurs also "smooths" the signal, as the instantaneous curve should abruptly change at the instant of contact. Of course, with a very small $\Delta T_a$, the two curves would be nearly identical. It should be noted, however, that, while the instantaneous stiffness is still computed by the algorithm at any moment between steps 3 and 4, its value should not be considered because the reconfiguration is not completed, and thus, would not have any signification. In other words, the values of $T_{a,0}$ and $\theta_{a,0}$ used to estimate $K_c$ (cf. Eq. (1)) must be $T_{a,c}$ and $\theta_{a,c}$ respectively. The instantaneous stiffnesses for the actual contact location at the moment of the contact and after the reconfiguration are also shown in Fig. 5. It can be noted that the measured stiffness is larger than it should be, but it is still slightly smaller than the expected stiffness at the new contact location reached at the end of the reconfiguration (this time for a $\Delta T_a = 0.2$ N). In this case, the algorithm still makes a precise approximation, with an error of less than 1 %.

To further the analysis, the next step is to quantify the effect of the curvature and the increase $\Delta T_a$ on the

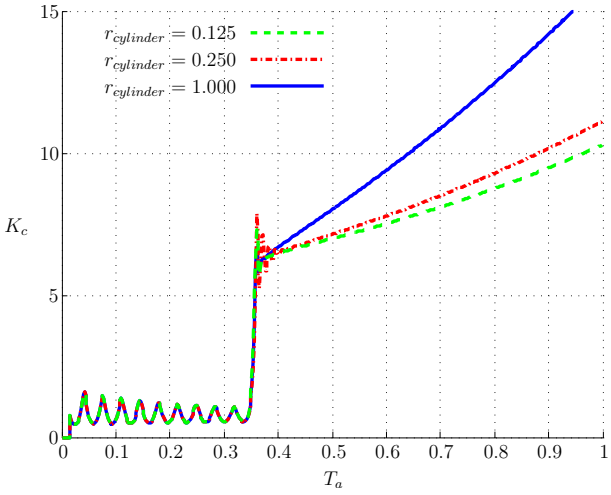


Fig. 6. Instantaneous stiffness for contacts on cylinders with different radii obtained with a dynamic solution package

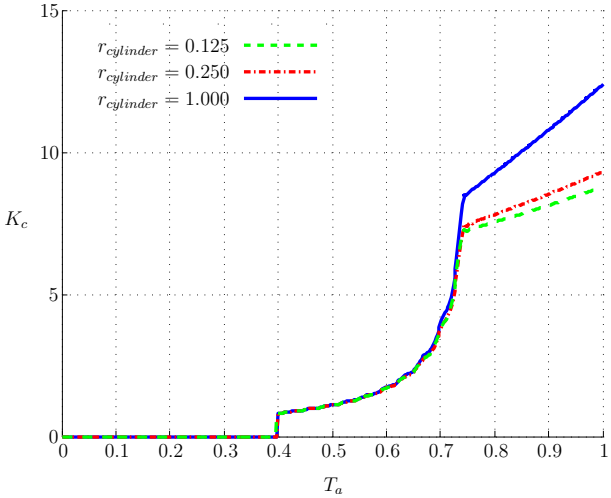


Fig. 7. PTS output for cylinder with different radii and a constant actuation torque needed for the measurement reconfiguration $\Delta T_a$

precision of the algorithm by testing different values.

### 3.3. Effect of the Curvature

To determine the effect of the curvature on the PTS algorithm, simulations using the DSP were established with several cylinders of different radii and the results are shown in Fig. 6. The evolution of the instantaneous stiffness for three different cylinders which are positioned to come into contact with the finger at the same location are presented. The data is numerically obtained, which explains the oscillations before the contact and the peak when it occurs. The instantaneous stiffness computed by the PTS algorithm when those signals are used is shown in Fig. 7. As can be seen, the impact of the curvature of the object on the measured instantaneous stiffness is limited, which can be explained by the quasi-exponential nature of the $k_2$-$K_c$ curve (see [12] for an example). Indeed, an error on $K_c$ usually leads to a smaller error on the algorithm's estimation of the contact location. Furthermore, experiments made with the previously presented prototype show a mean error on the contact location of 7.3 % with a standard deviation of 6.0 % (cf. [12]). Thus, knowing that for the largest cylinder tested (with a diameter 2.6 times the length of the distal phalanx) the maximum value of the error on the estimation is 9.6 %, one can conclude that the impact of the curvature of the object is limited compared to other phenomena causing deviations on the estimation such as friction in the transmission mechanism. To validate the simulations, several experimental tests were done with two different cylinders, one with a significantly larger diameter, to verify that the curvature's effect remains limited. Indeed, as it can be seen in Table 2, no clear correlation was detected, the deviation of the estimation from the actual contact location remaining in nearly all cases within the standard range also obtained with vertex (sharp) contact points.

| | Estimated contact location $\hat{k}_2/l_2$ | | |
|---|---|---|---|
| $k_2/l_2$ | $d_{cyl_1} = 0.5$ cm | $d_{cyl_2} = 75$ cm | difference |
| 0.11 | 0.05 | 0.07 | 2 % |
| 0.56 | 0.60 | 0.73 | 13 % |
| 0.50 | 0.44 | 0.49 | 5 % |
| 0.74 | 0.87 | 0.77 | -10 % |

Table 2. Experiments with two different cylinders

### 3.4. Variations of $\Delta T_a$

If one varies the reconfiguration torque increase to see its effect on the precision of the algorithm, it can be shown that it also remains very limited, as illustrated in Fig. 8. In this figure, the horizontal solid blue line represents the initial contact location, which is always the same (step 3 in Fig. 2) to be able to compare the results. On the other hand, the second blue curve represents the contact location after the reconfiguration (step 4 in Fig. 2) as a function of the chosen $\Delta T_a$. With the simulations performed, the relative error between the actual contact location after the reconfiguration and the estimation itself remains smaller than 3 %. This level is well below the habitual mean and standard deviation of errors as previously mentioned. While the effect of $\Delta T_a$ increases with the latter, a large $\Delta T_a$ is not needed for the algorithm to work. Therefore, if the reconfiguration torque increase has an impact on the algorithm's precision in theory, it is impossible to quantify it in practice without a better experimental setup where observable deviations caused by phenomena such as friction are eliminated.

A final experimental test was done with a cylinder with a diameter equal to 1 to see how a small $\Delta T_a$ could impact the PTS estimation. In this test, the variables $\theta_a$ and $T_a$ were measured and are illustrated in Fig. 9. One can see that there are perturbations initially when contact is made with the object. This is caused by the

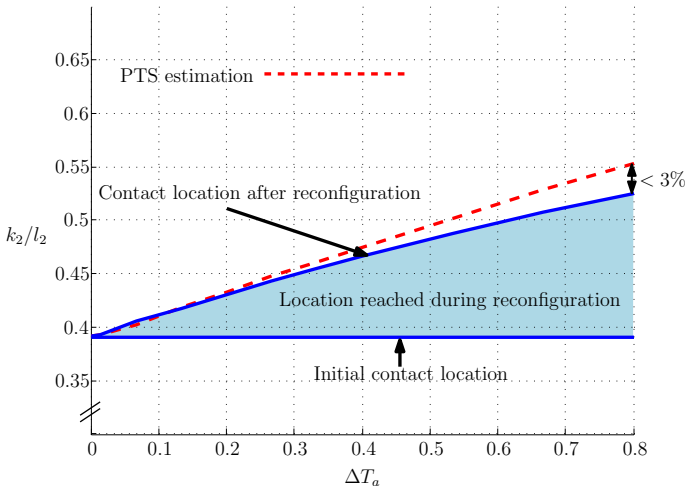


Fig. 8. PTS algorithm output for different $\Delta T_a$ (the location $k_2$, the configuration prior the instant of the contact, and the unitary diameter of the object are the same for every value tested)

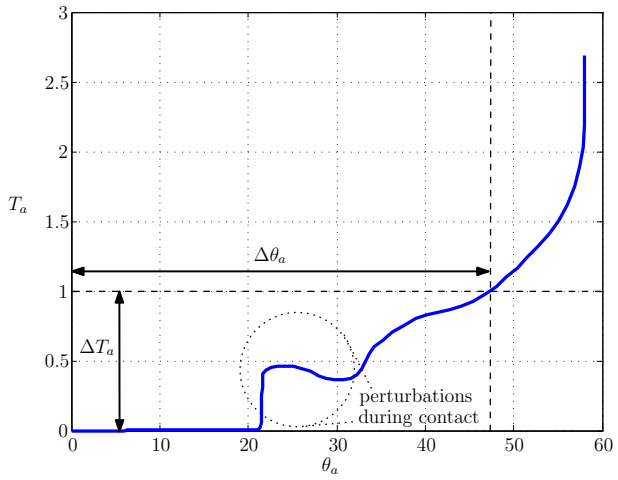


Fig. 9. Evolution of $T_a$ and $\theta_a$ during an experiment

impact between the two bodies and friction in the mechanism. First, while $T_a$ increases, the mechanism does not move. After a threshold is reached, motion resumes but the system is subjected to small oscillations. It finally reaches a stage where $\theta_a$ and $T_a$ increases as predicted. Therefore, it is important to avoid a torque increase too small, which might lead to a wrong estimation of the contact location.

## 4. CONCLUSIONS

Tactile sensing is becoming almost mandatory in many applications of robotics grippers and hands. However, conventional extrinsic tactile sensors typically attached to the surface of the robot suffer many drawbacks, including the sensitivity to several phenomena, complexity, and important costs. In this paper, practical consideration about an alternative tactile sensing method based on the stiffness of the mechanism, as seen at the actuator, are presented. Therefore, the curvature of the object and the reconfiguration needed for the algorithm to work were investigated. It was shown that while an effect is observable, the impact is not significant compared to other deviation causes such as internal friction. Indeed, for a $\Delta T_a$ within reasonable

limits, the shift caused by the algorithm in the measured stiffness closely follows the instantaneous stiffness of the new contact location after reconfiguration. However, the value of $\Delta T_a$ should be carefully chosen to avoid other phenomena, such as measurement noise immediately after the initial contact and a subsequent one before the PTS estimation is made. These findings suggest that while some hypotheses and simplification were made to obtain the model behind the PTS algorithm, they do not have a significant impact on the accuracy of the method in practical scenarios. Other possible limitations, however, such as the stiffness of the object grasped and simultaneous contacts, must still be studied. Future work will focus on feature extraction with active touch combined with proprioceptive tactile sensing.

## REFERENCES


1. Tiwana, M.I., Redmond, S.J. and Lovell, N.H. "A review of tactile sensing technologies with applications in biomedical engineering." *Sensors and Actuators A: Physical*, Vol. 179, pp. 17–31, 2012.
2. Dahiya, R.S. and Valle, M. "Tactile Sensing: Definitions and Classification." pp. 13–17. Springer Netherlands. DOI: 10.1007/978-94-007-0579-1_2, 2013.
3. Tegin, J. and Wikander, J. "Tactile sensing in intelligent robotic manipulation – a review." *Industrial Robot: An International Journal*, Vol. 32, No. 1, pp. 64–70. ISSN 0143-991X. doi:10.1108/01439910510573318, 02 2005.
4. Bicchi, A., Salisbury, J.K. and Dario, P. "Augmentation of grasp robustness using intrinsic tactile sensing." In "Proceedings, 1989 International Conference on Robotics and Automation," pp. 302–307 vol.1. doi: 10.1109/ROBOT.1989.100005, May 1989.
5. Backus, S. and Dollar, A. "Robust, inexpensive resonant frequency based contact detection for robotic manipulators." In "2012 IEEE International Conference on Robotics and Automation (ICRA)," pp. 1514–1519. Saint Paul, Minnesota, USA. doi:10.1109/ICRA.2012.6225152, May 2012.
6. Huber, M. and Grupen, R.A. "2-D Contact Detection and Localization Using Proprioceptive Information." *IEEE Transactions on Robotics and Automation*, Vol. 10, pp. 23–33, 1994.
7. Haidacher, S. and Hirzinger, G. "Contact point identification in multi-fingered grasps exploiting kinematic constraints." In "Proc. IEEE International Conference on Robotics and Automation," Vol. 2. Washington, May 2002.
8. Koonjul, G.S., Zeglin, G.J. and Pollard, N.S. "Measuring Contact Points from Displacements with a Compliant, Articulated Robot Hand." In "IEEE International Conference on Robotics and Automation (ICRA)," , 2011.
9. Kaneko, M. and Tanie, K. "Contact point detection for grasping an unknown object usign self-posture changeability." *IEEE Transactions on Robotics and Automation*, Vol. 10, No. 3, pp. 355–367, 1994.
10. Birglen, L., Laliberté, T. and Gosselin, C. *Underactuated Robotic Hands*. Springer Tracts in Advanced Robotics, 2008.
11. Fumagalli, M., Barrett, E., Stramigioli, S. and Carloni, R. "Analysis of an underactuated robotic finger with variable pinch and closure grasp stiffness." In "2016 IEEE International Conference on Advanced Intelligent Mechatronics (AIM)," pp. 365–370. doi:10.1109/AIM.2016.7576794, July 2016.
12. Belzile, B. and Birglen, L. "Stiffness Analysis of Underactuated Fingers and its Application to Proprioceptive Tactile Sensing." *IEEE/ASME Transactions on Mechatronics*, Vol. 21, No. 6, pp. 2672–2681. ISSN 1083-4435. doi:10.1109/TMECH.2016.2589546, 2016.
13. Belzile, B. and Birglen, L. "A compliant self-adaptive gripper with proprioceptive haptic feedback." *Autonomous Robots*, Vol. 36, No. 1-2, pp. 79–91, 2014.
14. Belzile, B. and Birglen, L. "Stiffness analysis of double tendon underactuated fingers." In "Robotics and Automation (ICRA), 2014 IEEE International Conference on," pp. 6679–6684. IEEE, Hong Kong, 2014.
15. Choi, H.R., Kim, J.H. and Oh, S.R. "Determination of three dimensional curvature of convex object via active touch." In "Proceedings. 1998 IEEE/RSJ International Conference on Intelligent Robots and Systems. Innovations in Theory, Practice and Applications (Cat. No.98CH36190)," Vol. 3, pp. 1652–1657 vol.3. doi: 10.1109/IROS.1998.724835, Oct 1998.